

Non-stabilizerness as a Diagnostic of Criticality and Exceptional Points in Non-Hermitian Spin Chains

Cătălin Pașcu Moca,^{1,2,3} Doru Sticlet,^{4,*} and Balázs Dóra^{2,3}

¹*Department of Physics, University of Oradea, 410087, Oradea, Romania*

²*Department of Theoretical Physics, Institute of Physics,*

Budapest University of Technology and Economics, Műegyetem rkp. 3, H-1111 Budapest, Hungary

³*MTA-BME Lendület "Momentum" Open Quantum Systems Research Group,*

Institute of Physics, Budapest University of Technology and Economics,

Műegyetem rkp. 3., H-1111, Budapest, Hungary

⁴*National Institute for R&D of Isotopic and Molecular Technologies, 67-103 Donat, 400293 Cluj-Napoca, Romania*

(Dated: October 21, 2025)

We investigate non-stabilizerness, also known as “magic,” to understand criticality and exceptional points in non-Hermitian quantum many-body systems. Our focus is on parity-time (\mathcal{PT}) symmetric spin chains, specifically the non-Hermitian transverse-field Ising and XX models. We calculate stabilizer Rényi entropies in their ground states using non-Hermitian matrix product state methods. Our findings show that magic exhibits unique and model-specific signs of phase transitions. In the Ising chain, it peaks along the regular Hermitian-like critical line but disappears across exceptional points. In contrast, in the XX chain, it reaches its maximum at the exceptional line where \mathcal{PT} symmetry is broken. Finite-size scaling reveals that these effects become more pronounced with larger systems, highlighting non-stabilizerness as a sensitive marker for both quantum criticality and non-Hermitian spectral degeneracies. We also investigate magic in momentum space for the XX model analytically and find that it reaches a minimum around exceptional points. Our results indicate that magic takes extremal values at the exceptional points and serves as a valuable tool for examining complexity, criticality, and symmetry breaking in non-Hermitian quantum matter.

INTRODUCTION

Non-Hermitian quantum systems have recently become a central theme in condensed matter physics, statistical mechanics, and quantum optics [1–3]. While Hermitian Hamiltonians guarantee real spectra and unitary dynamics, non-Hermitian Hamiltonians relax these constraints, allowing for complex energy spectra and non-unitary evolution [4–6]. Such models naturally arise in engineered photonic [7, 8] and cold-atom platforms [9, 10]. A particular subclass is formed by \mathcal{PT} symmetric Hamiltonians, which have real spectra in the \mathcal{PT} -symmetric regime, while crossing an exceptional point drives them into the \mathcal{PT} -broken phase, where eigenvalues appear in complex-conjugate pairs [11–15].

In parallel, quantum resource theory [16] has introduced new perspectives on many-body states, going beyond conventional order parameters and entanglement entropy [17–19]. One such concept is non-stabilizerness, often referred to as “magic” [20–25]. Magic quantifies the distance of a quantum state from the set of stabilizer states, which form the cornerstone of classically simulable quantum computation and stabilizer error correction codes [26–29]. A nonzero amount of magic is indispensable for universal fault-tolerant quantum computation, as it enables the realization of non-Clifford gates [30]. In many-body settings, magic has emerged as a sensitive probe of correlations, scrambling, and criticality, complementing entanglement measures and revealing new aspects of quantum complexity [22, 31–36].

Despite rapid progress in both directions, the inter-

section of non-Hermitian physics and non-stabilizerness remains largely unexplored. Non-Hermitian Hamiltonians are characterized by non-orthogonal eigenstates and exceptional points [37–40], raising fundamental questions about how quantum information measures behave in such contexts. For instance, does magic detect the onset of \mathcal{PT} -symmetry breaking and can non-stabilizerness provide a universal diagnostic of non-Hermitian quantum criticality or exceptional points?

In this work, we address these questions by investigating the stabilizer Rényi entropies in the ground state for two setups: for the non-Hermitian transverse-field Ising chain [41, 42] and for the non-Hermitian XX model [43, 44]. We demonstrate that non-stabilizerness offers a powerful tool to identify both conventional quantum critical points and non-Hermitian exceptional points. Our analysis shows that magic takes extremal values at the exceptional points, both in real space and in momentum space. These results position non-stabilizerness as a valuable addition to the growing toolbox of probes for non-Hermitian quantum matter.

Beyond these motivations, studying non-stabilizerness in non-Hermitian settings may also provide insights into the resource-based aspects of quantum computation under non-unitary evolution [45–47]. As experimental realizations of non-Hermitian systems become more common in various setups, understanding how magic works in these environments is directly relevant for near-term platforms.

STABILIZER RÉNYI ENTROPY

To quantify non-stabilizerness (“magic”) in the ground state, we work in the right-right (natural self-normal) basis using open boundary conditions (OBC). The ground state of the non-Hermitian Hamiltonian is computed using a Density Matrix Renormalization Group (DMRG) algorithm [48] adapted for non-Hermitian systems, as implemented in the ITensor library [49]. The right eigenstates are represented as matrix product states (MPS), with open boundary conditions [50]. Standard DMRG sweeps are modified to account for the non-Hermitian character of H , ensuring convergence to the correct right eigenvector. The ground state is identified as the state minimizing the real part of the energy.

Denoting the right ground state of the Hamiltonian H as $|\psi_R\rangle$, we define, for a subregion A of length ℓ , and its complement \bar{A} , the reduced density matrix

$$\rho_A^{RR} = \frac{\text{Tr}_{\bar{A}} (|\psi_R\rangle\langle\psi_R|)}{\langle\psi_R|\psi_R\rangle}, \quad (1)$$

which depends solely on the right eigenvector, and coincides with the standard Hermitian reduced density matrix when H is Hermitian. Expanding ρ_A^{RR} in the ℓ -qubit Pauli string basis \mathcal{P}_ℓ ,

$$\rho_A^{RR} = \frac{1}{2^\ell} \sum_{P \in \mathcal{P}_\ell} c_P P, \quad c_P = \text{Tr}(\rho_A^{RR} P), \quad (2)$$

the stabilizer 2-Rényi magic in the right-right basis is defined as

$$M_2^{RR}(A) = -\log_2 \left(\sum_{P \in \mathcal{P}_\ell} |c_P|^4 \right). \quad (3)$$

In practice, the coefficients c_P are efficiently obtained by evaluating expectation values of Pauli strings in the right-right basis.

To compute the stabilizer 2-Rényi magic M_2^{RR} , we employ a Metropolis-Hastings sampling scheme [51–53] within the MPS framework. The idea is to sample Pauli strings $P \in \mathcal{P}_\ell$ according to the weight $|c_P|^2$. Starting from an initial Pauli string, candidate updates are generated by single-qubit flips or local Pauli substitutions, and accepted with probability proportional to the ratio of $|c_P|^2$ for the new and old strings, ensuring convergence to the correct distribution [54]. In the MPS language [23], each evaluation of c_P is performed by contracting the MPS tensors in the RR basis with the corresponding Pauli operator on subsystem A . This approach allows for scalable estimation of M_2^{RR} in large L limit, where enumerating all 4^ℓ Pauli strings would be computationally prohibitive. To minimize the errors, we perform an average over several separate Markov chains.

We stress that stabilizer Rényi entropies provide infor-

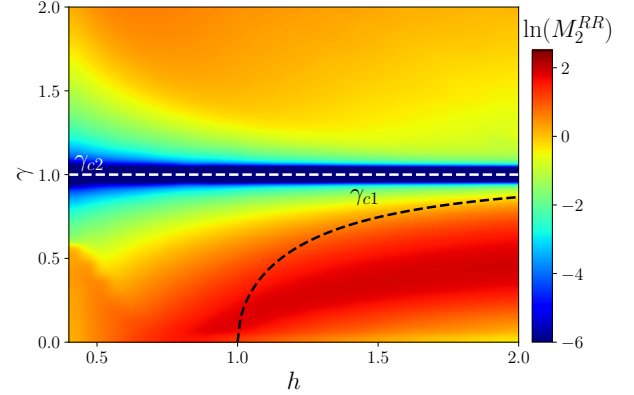


FIG. 1. Ground-state density plot of $M_2^{RR}(L)$. The dashed black and white lines indicate the theoretical critical lines γ_{c1} and γ_{c2} in the thermodynamic limit. Magic peaks along the Ising transition line and vanishes at the exceptional points across the phase diagram. System size is fixed to $L = 16$.

mation complementary to entanglement entropies. While entanglement captures correlations across bipartitions, magic measures the intrinsic non-classicality of the state in terms of its departure from stabilizer form. In non-Hermitian systems, this distinction becomes crucial: entanglement may survive even when eigenstates acquire non-orthogonal character, but magic can vanish if the state approaches a generalized stabilizer structure. Thus, analyzing M_2^{RR} reveals unique signatures of non-Hermitian quantum matter.

NON-HERMITIAN TRANSVERSE FIELD ISING MODEL

The one-dimensional non-Hermitian transverse-field Ising (NHTI) model [42], defined by

$$H = -J \sum_{j=1}^L \sigma_j^x \sigma_{j+1}^x + \sum_{j=1}^L h(\sigma_j^z + i\gamma\sigma_j^y), \quad (4)$$

extends the conventional Hermitian transverse-field Ising chain by introducing an imaginary field along the y direction. For $\gamma = 0$ the model reduces to the standard [55]. In this limit, it undergoes a second-order quantum phase transition between ferromagnetic (FM) and paramagnetic (PM) phase at $h = J$. When $\gamma \neq 0$, the Hamiltonian becomes non-Hermitian but retains \mathcal{PT} symmetry, ensuring that eigenvalues are either real or come in complex-conjugate pairs. The model is exactly solvable via a Jordan-Wigner transformation, which maps it to a non-Hermitian free-fermion problem [42].

For non-Hermitian Hamiltonians, the notion of a ground state is not uniquely defined due to the possibility of complex eigenvalues. In this work, we define the ground

state as the eigenstate with the smallest real part of the energy, providing a consistent convention for analyzing stabilizer Rényi entropy.

The ground state phase diagram in the (h, γ) plane reveals two distinct critical lines. The first critical line corresponds to the *ground-state Ising transition* in the \mathcal{PT} symmetric region [56] for $\gamma < 1$, occurring at

$$\gamma_{c1} = \sqrt{1 - (J/h)^2}. \quad (5)$$

The second critical is the *full \mathcal{PT} -transition* at $\gamma_{c2} = 1$, where the entire many-body spectrum changes from \mathcal{PT} -symmetric (real energies) to \mathcal{PT} -broken (complex energies), featuring second-order exceptional points [57]. The two critical lines as emerging in the thermodynamic limit, are indicated by the dashed lines in Fig. 1. By symmetry, the phase diagram extends naturally to negative values of both h and γ , covering the regions $h < 0$ and $\gamma < 0$ as well.

The FM and PM phases are separated by these critical lines, with \mathcal{PT} -symmetric regions hosting purely real energies and \mathcal{PT} -broken regions exhibiting finite imaginary parts in the spectrum [11]. The non-Hermitian character modifies the quasiparticle dispersion relation by introducing complex-valued energies, and this affects the dynamical correlations and observables. The interplay of the transverse field h and the non-Hermitian parameter γ provides a rich structure that we exploit to study non-stabilizerness.

The stabilizer 2-Rényi magic M_2^{RR} in the ground state exhibits distinct features that reflect the underlying phase structure of the model. As shown in Fig. 1, M_2^{RR} peaks along the Ising transition line, indicating enhanced non-stabilizerness at the quantum critical point, and vanishes at the exceptional points where the system undergoes a \mathcal{PT} -symmetry-breaking transition. The position of the maximum in M_2^{RR} shows a slight deviation from the exact critical line γ_{c1} , which we attribute to finite-size effects. In contrast, at the \mathcal{PT} -transition, M_2^{RR} vanishes exactly, independent of the system size.

This can be understood from the similarity transformation [42], which consist of a rotation around σ^x and maps the non-Hermitian Hamiltonian onto a Hermitian one. The rotation results in a Hermitian transverse field Ising chain with an effective transverse field as $h\sqrt{1 - \gamma^2}$. At the exceptional point with $\gamma = 1$, the transverse field vanishes in the effective Hermitian model and it reduces to a simple Ising chain. Its ground state is a fully polarized ferromagnet with $\langle \sigma_j^x \rangle = \pm 1$. The ground state wavefunction of the non-Hermitian model is obtained by an inverse similarity transformation on the wavefunction, which means an inverse rotation around σ^x . However, since the Hermitian ground state is fully polarized in the x direction in spin space, it remains intact by the inverse similarity transformation and the ground state of the non-Hermitian Ising model along the exceptional line is the

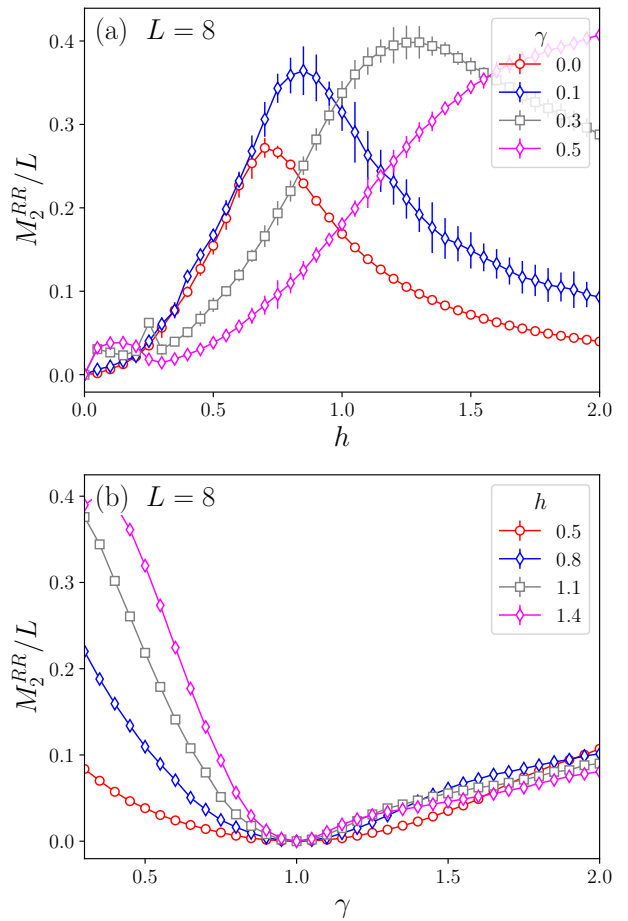


FIG. 2. (a) Horizontal cuts through the phase diagram at several values of γ in the \mathcal{PT} -symmetric regime, showing that M_2^{RR} peaks at the Ising transition. (b) Vertical cuts along the non-Hermitian parameter γ for different external magnetic fields, illustrating that magic reaches its maximum at the Ising transition and vanishes at the exceptional point $\gamma = 1$.

fully ferromagnetic state. This is a stabilizer state and its magic is zero.

By analyzing horizontal and vertical cuts through the phase diagram (Fig. 2), one clearly observes that magic reaches its maximum at the critical line γ_{c1} separating the ferromagnetic and paramagnetic phases, while it drops to zero at the full \mathcal{PT} -transition line $\gamma_{c2} = 1$.

The behavior of M_2^{RR} as a function of system size provides additional insight. As shown in Fig. 3, increasing the chain length sharpens the features of M_2^{RR} near the critical lines, making the peaks at the Ising transition more pronounced. This scaling indicates that the maximum of M_2^{RR} converges toward the true critical line γ_{c1} in the thermodynamic limit, while the drop to zero at $\gamma_{c2} = 1$ becomes increasingly abrupt.

This behavior demonstrates that M_2^{RR} provides a direct and sensitive probe of both conventional quantum phase transitions and non-Hermitian exceptional points, allow-

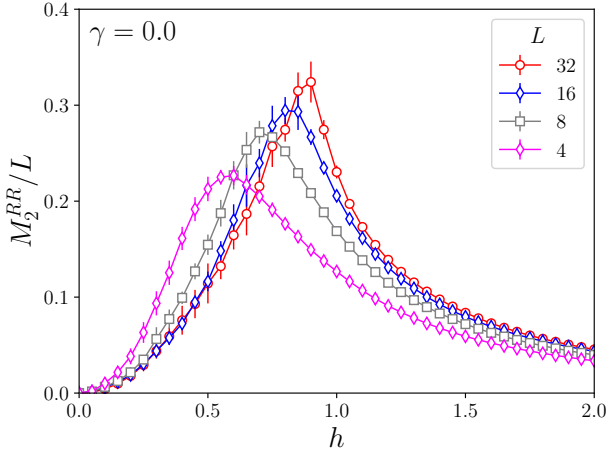


FIG. 3. Scaling of M_2^{RR} with system size. As the system size increases, the location of the transition becomes sharper and better resolved.

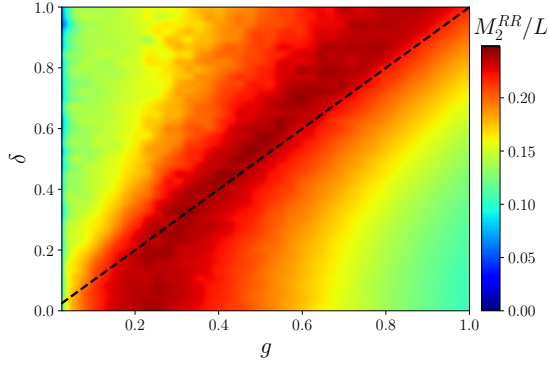


FIG. 4. Ground-state density plot of $M_2^{RR}(L)$. The dashed black lines indicate the theoretical exceptional points line. Magic peaks along the \mathcal{PT} exceptional line. The system size is $L = 16$.

ing one to reconstruct the ground-state phase diagram of the system from the pattern of magic alone.

NON-HERMITIAN XX MODEL

The non-Hermitian XX model provides a complementary setting to investigate the interplay between \mathcal{PT} symmetry and non-stabilizerness. We contrast here the magic computed in real space lattices with OBC, and momentum space magic [58]. In both cases, non-stabilizerness takes extremal values at the exceptional points in the phase diagram.

Real space non-stabilizerness

The starting point is a non-Hermitian tight-binding model for spinless fermions [44, 59], endowed with \mathcal{PT} symmetry, and described by the Hamiltonian

$$H = \sum_{j=1}^{L-1} [J + i(-1)^j \delta] (c_j^\dagger c_{j+1} + \text{H.c.}) + 2g \sum_{j=1}^L (-1)^j c_j^\dagger c_j, \quad (6)$$

with J , the uniform exchange coupling, δ , a staggered non-Hermitian component, and g , a staggered longitudinal field. Diagonalization yields a two-band spectrum,

$$E_\pm(k) = \pm 2\sqrt{(J^2 + \delta^2) \cos^2 k + g^2 - \delta^2}, \quad (7)$$

with momenta $k \in [0, \pi]$. For $g > \delta$, the spectrum is real, and the system lies in the \mathcal{PT} -symmetric phase. At the critical line $g = \delta$, the bands touch at $k = \pi/2$, signaling a \mathcal{PT} -symmetric exceptional point with linear dispersion. At half-filling, the exceptional points lies at the Fermi level. For $g < \delta$, the spectrum becomes complex near $k = \pi/2$, indicating entry into the \mathcal{PT} -broken regime where eigenvalues occur in conjugate pairs.

In order to study non-stabilizerness, we map the fermionic Hamiltonian to a spin (qubit) model. Under a Jordan-Wigner transformation, Eq. (6) maps to a non-Hermitian XX chain with staggered complex exchange and staggered transverse field [43],

$$H_{\text{XX}} = \sum_{j=1}^{L-1} [J + i(-1)^j \delta] (\sigma_j^+ \sigma_{j+1}^- + \text{H.c.}) + g \sum_{j=1}^L (-1)^j \sigma_j^z, \quad (8)$$

with $\sigma^\pm = \frac{1}{2}(\sigma^x \pm i\sigma^y)$. Its phases remain the same: a gapped \mathcal{PT} -symmetric phase, a critical line of exceptional points at $g = \delta$, and a \mathcal{PT} -broken phase with complex spectrum. This structure parallels that of the non-Hermitian Ising chain, and provides an alternative platform where stabilizer Rényi entropies can be employed to probe both conventional criticality and non-Hermitian exceptional points.

The stabilizer 2-Rényi magic M_2^{RR} in the ground state of the XX model displays distinctive signatures that mirror this phase structure. As shown in Fig. 4, M_2^{RR} develops pronounced ridges along the exceptional line $g = \delta$, reaching its maximum value close to the \mathcal{PT} -symmetric exceptional points. In contrast to the transverse-field Ising case, where magic vanishes at the exceptional transition, here the non-stabilizerness is maximized at the onset of \mathcal{PT} -symmetry breaking. This highlights the model dependence of magic as a diagnostic: while in the Ising chain it signals conventional quantum criticality, in the XX model it is sensitive to exceptional points. Horizontal cuts through the phase diagram (Fig. 5) confirm this behavior, showing peaks of M_2^{RR} pinned to the exceptional

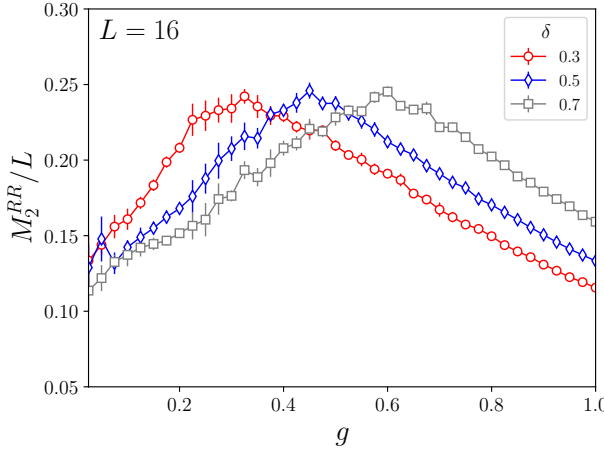


FIG. 5. Horizontal cuts through the phase diagram at several values of δ showing that M_2^{RR} peaks at the exceptional point.

line.

Momentum space non-stabilizerness

A complementary perspective on the non-Hermitian model (6) consists in determining its non-stabilizerness in momentum space, \mathcal{M}_2^{RR} [58]. The XX model becomes analytically solvable in momentum space, where it is diagonalized in separate k sectors, and the total magic becomes a trivial sum of few-qubit results from each sector. To determine a momentum-space spin Hamiltonian, we start with the fermionic Hamiltonian (6) with periodic boundary conditions, in momentum space,

$$H = \sum_{k=0}^{\pi} C_k^\dagger H_k C_k, \quad \frac{H_k}{2} = \begin{pmatrix} J \cos k & g + \delta \sin k \\ g - \delta \sin k & -J \cos k \end{pmatrix}, \quad (9)$$

with $C_k^\dagger = (c_k^\dagger, c_{k-\pi}^\dagger)$. Then, we perform a Jordan-Wigner transformation, mapping fermion to spin operators. E.g., the annihilation operators are represented as

$$c_k = \exp \left[i \frac{\pi}{2} \sum_{q \in \mathcal{D}_k} (\sigma_q^z + \sigma_q^0) \right] \sigma_k^-, \quad (10)$$

with momenta q in the set $\mathcal{D}_k = [-\pi, k-\pi) \cup [0, k)$. Thus, the number operator is $c_k^\dagger c_k = \sigma_k^+ \sigma_k^- \equiv \frac{1}{2}(\sigma_k^z + \sigma_k^0)$, with σ_k^0 the 2×2 identity matrix. Inside the Jordan-Wigner string, the order of momenta is in pairs $(q-\pi, q)$, such that the Jordan-Wigner transformations reads explicitly

$$c_k = \left(\prod_{q \in [0, k)} \sigma_{q-\pi}^z \sigma_q^z \right) \sigma_k^-, \quad (11)$$

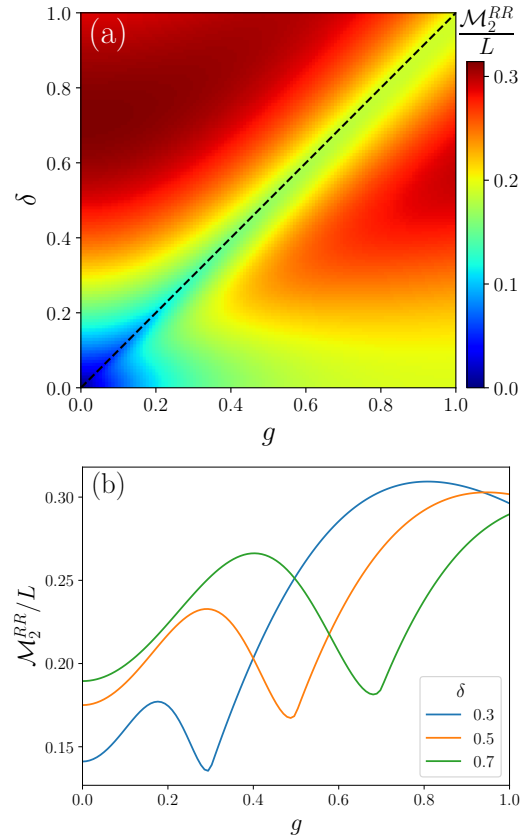


FIG. 6. (a) Ground-state magic density \mathcal{M}_2^{RR}/L in momentum space for the XX model, using a mesh of $L = 800$ momenta in $[0, \pi)$. The dashed line indicates the exceptional line in parameter space. (b) Horizontal cuts through the phase diagram at several values of δ showing that \mathcal{M}_2^{RR}/L has a local minimum at the exceptional points.

with momenta q increasing from 0 to k . The transformation yields the momentum space Hamiltonian

$$H = \sum_{k \in [0, \pi)} 2(g + \delta \sin k) \sigma_k^+ \sigma_{k-\pi}^- + 2(g - \delta \sin k) \sigma_k^- \sigma_{k-\pi}^+ + J \cos k (\sigma_k^z - \sigma_{k-\pi}^z). \quad (12)$$

Since only k and $k - \pi$ momenta remain coupled in this Hamiltonian, it is meaningful to represent it in the two-qubit basis $\{|0\rangle_{k-\pi} \otimes |0\rangle_k, |1\rangle_{k-\pi} \otimes |1\rangle_k, |0\rangle_{k-\pi} \otimes |1\rangle_k, |1\rangle_{k-\pi} \otimes |0\rangle_k\}$. To simplify the notation, we denote $|0\rangle_{k-\pi} \otimes |0\rangle_k$ as $|00\rangle_k$, etc. The qubit states are defined such that $\sigma_k^z |0\rangle_k = -|0\rangle_k$ and $\sigma_k^z |1\rangle_k = |1\rangle_k$. Since the Hamiltonian conserves the number of spin excitations, it assumes for each momentum k a 2×2 matrix form in the reduced basis $\{|01\rangle_k, |10\rangle_k\}$, where it is represented by H_k from Eq. (9).

The ground state of the system is a product state in momentum space $|\Phi\rangle = \bigotimes_{k \in [0, \pi)} |\phi_k\rangle$, with

$$|\phi_k\rangle = \alpha_k |01\rangle_k + \beta_k |10\rangle_k. \quad (13)$$

The ground state is defined as the state with the lowest real energy of H_k for each momentum k . Then, its non-stabilizerness depends entirely on the coefficients α_k and β_k , and the total magic is obtained by summing the contributions from each momentum sector. The resulting diagram for the magic density \mathcal{M}_2^{RR}/L in $g-\delta$ plane are shown in Fig. 6(a), where L is the number of momenta in the Brillouin zone $[0, \pi]$. Additionally, a few cuts through the phase diagram at fixed δ are shown in Fig. 6(b) illustrating that at exceptional points, non-stabilizerness reaches a local minimum. As expected, near the $g = \delta = 0$ point, the magic density vanishes, since the ground state is a stabilizer state, a product of eigenstates of σ^z , as evident from Eq. (12). Moving along the line of exceptional points $g = \delta$, the magic density increases until it saturates at some finite value. On the exceptional line, the qubit in each momentum sector rotates in the $x-z$ plane, simplifying the analysis. Thus, the saturation value on the exceptional line is found analytically,

$$\lim_{g \rightarrow \infty} \frac{\mathcal{M}_2^{RR}}{L} = -\frac{1}{\pi} \int_0^\pi dk \log_2 \frac{1 + \sin^4 k + \cos^4 k}{2} = \log_2(112 - 64\sqrt{3}) \approx 0.2. \quad (14)$$

In Fig. 7, we show the rapid convergence of magic density to the analytical limit when increasing $g = \delta$. Moreover, in the inset Fig. 7, we show the momentum-resolved magic for several values on the exceptional line, demonstrating that exactly at the exceptional point $k = \pi/2$, the magic vanishes, as the qubit aligns along the z axis. Interestingly, as the qubit state rotates in the $x-z$ plane, it passes through a second magic minimum, where it becomes a stabilizer state, being completely aligned along the x axis.

Importantly, the magic density attains a minimum along the exceptional line in the $g-\delta$ phase diagram. This behavior contrasts sharply with that of the real-space magic, which instead peaks at the exceptional line. Such a discrepancy arises from the basis dependence of magic. Nonetheless, in both representations, the extreme values of magic reliably signal the onset of \mathcal{PT} -symmetry breaking at the exceptional points.

CONCLUSIONS

In this work, we have explored non-stabilizerness, quantified by stabilizer Rényi entropies, as a diagnostic tool for non-Hermitian quantum many-body systems. Using the non-Hermitian transverse-field Ising chain and the non-Hermitian XX chain as models, we analyzed ground-state properties across their respective phase diagrams.

Our results show that magic provides a clear signature of the quantum phase transitions in non-Hermitian systems. In the Ising chain, \mathcal{M}_2^{RR} peaks along the critical line, signaling the presence of non-classical resources at the transition, and vanishes across exceptional points,

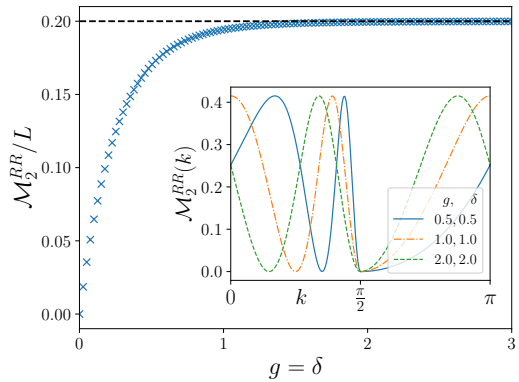


FIG. 7. Magic density along the exceptional line $g = \delta$ rapidly saturates to the (dashed line) analytical limit (14). The inset shows the momentum-resolved magic for several values on the exceptional line. The magic is zero at the exceptional point $k = \pi/2$, while an additional magic minimum occurs at $k < \pi/2$ when the qubit orients itself along x axis.

reflecting the coalescence of eigenstates.

By contrast, in the real-space XX chain M_2^{RR} is maximized along the exceptional line. We have also analyzed magic in momentum space for the XX model and found that it reaches a minimum at exceptional points, in contrast to its real space counterpart. This clearly highlights the essential basis dependence of the magic.

Finite-size scaling further confirms that these features sharpen with increasing system size, establishing M_2^{RR} as a reliable probe of non-Hermitian criticality.

Taken together, our findings demonstrate that non-stabilizerness captures essential equilibrium features of non-Hermitian quantum matter in ways that complement traditional measures such as entanglement entropy. Magic thus emerges as a versatile addition to the toolbox for characterizing resource properties in non-Hermitian systems.

Looking ahead, it will be interesting to extend these ideas to disordered or non-equilibrium systems and experimental platforms where non-Hermitian physics and quantum information concepts meet.

ACKNOWLEDGMENTS

This work received financial support from CNCS/CCCDI-UEFISCDI, under projects number PN-IV-P1-PCE-2023-0159, PN-IV-P1-PCE-2023-0987, PN-IV-P8-8.3-PM-RO-FR-2024-0059, and by the “Nucleu” Program within the PNCDI 2022-2027, Romania, carried out with the support of MEC, project no. 27N/03.01.2023, component project code PN 23 24 01 04. This research was also supported by the National Research, Development and Innovation Office - NKFH within the Quantum Technology National Excellence

Program (Project No. 2017-1.2.1-NKP-2017-00001), K134437, K142179 by the BME-Nanotechnology FIKP grant (BME FIKP-NAT). We acknowledge the Digital Government Development and Project Management Ltd. for awarding us access to the Komondor HPC facility based in Hungary.

* doru.sticlet@itim-cj.ro

- [1] N. Moiseyev, *Non-Hermitian Quantum Mechanics* (Cambridge University Press, Cambridge, 2011).
- [2] Y. Ashida, Z. Gong, and M. Ueda, Non-Hermitian physics, *Adv. Phys.* **69**, 249–435 (2020).
- [3] C. Wang, Z. Fu, W. Mao, J. Qie, A. D. Stone, and L. Yang, Non-Hermitian optics and photonics: From classical to quantum, *Adv. Opt. Photon.* **15**, 442 (2023).
- [4] I. Rotter, A non-Hermitian Hamilton operator and the physics of open quantum systems, *J. Phys. A: Math. Theor.* **42**, 153001 (2009).
- [5] F. Roccati, G. M. Palma, F. Ciccarello, and F. Bagarello, Non-Hermitian physics and master equations, *Open Syst. Inf. Dyn.* **29**, 2250004 (2022).
- [6] A. Gómez-León, T. Ramos, A. González-Tudela, and D. Porras, Bridging the gap between topological non-Hermitian physics and open quantum systems, *Phys. Rev. A* **106**, L011501 (2022).
- [7] Q. Yan, B. Zhao, R. Zhou, R. Ma, Q. Lyu, S. Chu, X. Hu, and Q. Gong, Advances and applications on non-Hermitian topological photonics, *Nanophotonics* **12**, 2247 (2023).
- [8] A. Li, H. Wei, M. Cotrufo, W. Chen, S. Mann, X. Ni, B. Xu, J. Chen, J. Wang, S. Fan, C.-W. Qiu, A. Alù, and L. Chen, Exceptional points and non-Hermitian photonics at the nanoscale, *Nat. Nanotechnol.* **18**, 706 (2023).
- [9] L. Li, C. H. Lee, and J. Gong, Topological switch for non-Hermitian skin effect in cold-atom systems with loss, *Phys. Rev. Lett.* **124**, 250402 (2020).
- [10] Y. Luo, N. Liu, and J.-Q. Liang, Quantum phase transition and exceptional points of a non-hermitian hamiltonian for cold atoms in a dissipative optical cavity with nonlinear atom-photon interactions, *Phys. Rev. A* **110**, 063320 (2024).
- [11] A. Mostafazadeh, Pseudo-Hermiticity versus PT symmetry: The necessary condition for the reality of the spectrum of a non-Hermitian Hamiltonian, *J. Math. Phys.* **43**, 205–214 (2002).
- [12] A. Mostafazadeh, Exact pt-symmetry is equivalent to hermiticity, *J. Phys. A: Math. Gen.* **36**, 7081 (2003).
- [13] L. Feng, R. El-Ganainy, and L. Ge, Non-Hermitian photonics based on parity-time symmetry, *Nat. Photonics* **11**, 752 (2017).
- [14] S. Longhi, Parity-time symmetry meets photonics: A new twist in non-Hermitian optics, *Europhys. Lett.* **120**, 64001 (2018).
- [15] C. M. Bender and D. W. Hook, \mathcal{PT} -symmetric quantum mechanics, *Rev. Mod. Phys.* **96**, 045002 (2024).
- [16] E. Chitambar and G. Gour, Quantum resource theories, *Rev. Mod. Phys.* **91**, 025001 (2019).
- [17] V. Veitch, S. A. Hamed Mousavian, D. Gottesman, and J. Emerson, The resource theory of stabilizer quantum computation, *New J. Phys.* **16**, 013009 (2014).
- [18] M. Howard and E. Campbell, Application of a resource theory for magic states to fault-tolerant quantum computing, *Phys. Rev. Lett.* **118**, 090501 (2017).
- [19] Z.-W. Liu and A. Winter, Many-body quantum magic, *PRX Quantum* **3**, 020333 (2022).
- [20] L. Leone, S. F. E. Oliviero, and A. Hamma, Stabilizer Rényi entropy, *Phys. Rev. Lett.* **128**, 050402 (2022).
- [21] J. Odavić, M. Viscardi, and A. Hamma, Stabilizer entropy in nonintegrable quantum evolutions, *Phys. Rev. B* **112**, 104301 (2025).
- [22] P. S. Tarabunga, Critical behaviors of non-stabilizerness in quantum spin chains, *Quantum* **8**, 1413 (2024).
- [23] T. Haug and L. Piroli, Stabilizer entropies and nonstabilizerness monotones, *Quantum* **7**, 1092 (2023).
- [24] A. Sinibaldi, A. F. Mello, M. Collura, and G. Carleo, *Non-stabilizerness of neural quantum states* (2025), arXiv:2502.09725 [quant-ph].
- [25] J. Huang, X. Qian, and M. Qin, Nonstabilizerness entanglement entropy: A measure of hardness in the classical simulation of quantum many-body systems with tensor network states, *Phys. Rev. A* **112**, 012425 (2025).
- [26] D. Gottesman, *Stabilizer codes and quantum error correction* (California Institute of Technology, 1997).
- [27] S. Aaronson and D. Gottesman, Improved simulation of stabilizer circuits, *Phys. Rev. A* **70**, 052328 (2004).
- [28] J. Dehaene and B. De Moor, Clifford group, stabilizer states, and linear and quadratic operations over GF(2), *Phys. Rev. A* **68**, 042318 (2003).
- [29] S. Masot-Llima and A. Garcia-Saez, Stabilizer tensor networks: Universal quantum simulator on a basis of stabilizer states, *Phys. Rev. Lett.* **133**, 230601 (2024).
- [30] B. J. Brown, A fault-tolerant non-Clifford gate for the surface code in two dimensions, *Science Advances* **6**, 10.1126/sciadv.aay4929 (2020).
- [31] S. F. E. Oliviero, L. Leone, and A. Hamma, Magic-state resource theory for the ground state of the transverse-field Ising model, *Phys. Rev. A* **106**, 042426 (2022).
- [32] J. Odavić, T. Haug, G. Torre, A. Hamma, F. Franchini, and S. M. Giampaolo, Complexity of frustration: A new source of non-local non-stabilizerness, *SciPost Phys.* **15**, 131 (2023).
- [33] D. Sticlet, B. Dóra, D. Szombathy, G. Zaránd, and C. P. Moca, *Non-stabilizerness in open XXZ spin chains: Universal scaling and dynamics* (2025), arXiv:2504.11139 [quant-ph].
- [34] M. Sarkis and A. Tkatchenko, *Are molecules magical? Non-stabilizerness in molecular bonding* (2025), arXiv:2504.06673 [quant-ph].
- [35] C. P. Moca, D. Sticlet, B. Dóra, A. Valli, D. Szombathy, and G. Zaránd, *Non-stabilizerness generation in a multi-particle quantum walk* (2025), arXiv:2504.19750 [quant-ph].
- [36] S. Bera and M. Schirò, *Non-stabilizerness of Sachdev-Ye-Kitaev model* (2025), arXiv:2502.01582 [quant-ph].
- [37] W. D. Heiss, Exceptional points of non-Hermitian operators, *J. Phys. A: Math. Gen.* **37**, 2455–2464 (2004).
- [38] M. V. Berry, Physics of nonhermitian degeneracies, *Czech. J. Phys.* **54**, 1039 (2004).
- [39] F. Minganti, A. Miranowicz, R. W. Chhajlany, and F. Nori, Quantum exceptional points of non-Hermitian Hamiltonians and Liouvillians: The effects of quantum jumps, *Phys. Rev. A* **100**, 062131 (2019).
- [40] K. Ding, C. Fang, and G. Ma, Non-Hermitian topology and exceptional-point geometries, *Nat. Rev. Phys.* **4**,

745–760 (2022).

[41] G. A. Starkov, M. V. Fistul, and I. M. Eremin, Quantum phase transitions in non-Hermitian PT-symmetric transverse-field Ising spin chains, *Ann. Phys. (N. Y.)* **456**, 169268 (2023).

[42] C.-Z. Lu, X. Deng, S.-P. Kou, and G. Sun, Many-body phase transitions in a non-Hermitian Ising chain, *Phys. Rev. B* **110**, 014441 (2024).

[43] Y. Ashida, S. Furukawa, and M. Ueda, Parity-time-symmetric quantum critical phenomena, *Nat. Commun.* **8**, 10.1038/ncomms15791 (2017).

[44] B. Dóra, D. Sticlet, and C. P. Moca, Correlations at PT-symmetric quantum critical point, *Phys. Rev. Lett.* **128**, 146804 (2022).

[45] S. Fortin, F. Holik, and L. Vanni, Non-unitary evolution of quantum logics, in *Non-Hermitian Hamiltonians in Quantum Physics: Selected Contributions from the 15th International Conference on Non-Hermitian Hamiltonians in Quantum Physics, Palermo, Italy, 18–23 May 2015* (Springer, 2016) pp. 219–234.

[46] C. P. Williams, Probabilistic nonunitary quantum computing, in *Quantum Information and Computation II*, Vol. 5436 (SPIE, 2004) pp. 297–306.

[47] X. Turkeshi and M. Schirò, Entanglement and correlation spreading in non-Hermitian spin chains, *Phys. Rev. B* **107**, L020403 (2023).

[48] S. R. White, Density matrix formulation for quantum renormalization groups, *Phys. Rev. Lett.* **69**, 2863 (1992).

[49] M. Fishman, S. R. White, and E. M. Stoudenmire, The ITensor software library for tensor network calculations, *SciPost Phys. Codebases* **4** (2022).

[50] U. Schollwöck, The density-matrix renormalization group in the age of matrix product states, *Ann. Phys. (N. Y.)* **326**, 96 (2011).

[51] S. Chib and E. Greenberg, Understanding the Metropolis-Hastings algorithm, *Amer. Statist.* **49**, 327 (1995).

[52] C. P. Robert and G. Casella, Metropolis-Hastings algorithms, in *Introducing Monte Carlo Methods with R* (Springer, 2009) pp. 167–197.

[53] G. O. Roberts and J. S. Rosenthal, Optimal scaling for various Metropolis-Hastings algorithms, *Statist. Sci.* **16**, 351 (2001).

[54] P. S. Tarabunga, E. Tirrito, T. Chanda, and M. Dalmonte, Many-body magic via Pauli-Markov chains—From criticality to gauge theories, *PRX Quantum* **4**, 040317 (2023).

[55] P. Pfeuty, The one-dimensional Ising model with a transverse field, *Ann. Phys.-New. York* **57**, 79 (1970).

[56] F. Yang, H. Wang, M.-L. Yang, C.-X. Guo, X.-R. Wang, G.-Y. Sun, and S.-P. Kou, Hidden continuous quantum phase transition without gap closing in non-Hermitian transverse Ising model, *New J. Phys.* **24**, 043046 (2022).

[57] An analysis of the excited states reveals the presence of the third critical line, in the \mathcal{PT} -broken regime ($\gamma > 1$), where the first and second excited states coalesce and acquire complex energies, again through second-order exceptional points.

[58] B. Dóra and C. Moca, Momentum space nonstabilizerness for the transverse field quantum ising model, *Phys. Rev. B* **112**, 125427 (2025).

[59] Y. Ashida and M. Ueda, Full-counting many-particle dynamics: Nonlocal and chiral propagation of correlations, *Phys. Rev. Lett.* **120**, 185301 (2018).